Υ suppression in a hadron gas

L. M. Abreu[*]
Instituto de Física, Universidade Federal da Bahia, Campus Universitário de Ondina, 40170-115, Bahia, Brazil

F. S. Navarra[†]
Instituto de Física, Universidade de São Paulo, Rua do Matão 1371, 05508-090 São Paulo, São Paulo, Brazil

M. Nielsen[‡]
Instituto de Física, Universidade de São Paulo, Rua do Matão 1371, 05508-090 São Paulo, São Paulo, Brazil
and SLAC Nacional Acelerator Laboratory, Stanford University, Stanford, California 94309, USA

(Received 13 August 2019; revised manuscript received 4 November 2019; published 9 January 2020)

In this work, we study the interactions of bottom mesons which lead to Υ production and absorption in hot hadronic matter. We use effective Lagrangians to calculate the Υ production cross section in processes such as $\bar{B}^{(*)} + B^{(*)} \to \Upsilon + (\pi, \rho)$ and also the Υ absorption cross section in the corresponding inverse processes. We update and extend previous calculations by Lin and Ko, introducing anomalous interactions. The obtained cross sections are used as input to solve the rate equation which allows us to follow the time evolution of the Υ multiplicity. In contrast to previous conjectures, our results suggest that the interactions in the hadron gas phase reduce the Υ abundance.

DOI: 10.1103/PhysRevC.101.014906

I. INTRODUCTION

One of the most interesting predictions of QCD is that strongly interacting matter undergoes a phase transition to a deconfined state at sufficiently high temperatures. The medium composed of quarks and gluons in this deconfined state is referred to as the quark-gluon plasma (QGP) and it has been observed in heavy-ion collisions at the Relativistic Heavy Ion Collider (RHIC) [1] and the Large Hadron Collider (LHC) [2].

Heavy quark bound states are believed to be reliable probes of the quark gluon plasma. In the QGP, once the heavy quarkonium states are formed, they are expected to unbind due to the strong interactions with partons in the medium through a QCD Debye screening mechanism [3,4]. Above a certain temperature, the more weakly bound states, such as $\Upsilon(3S)$, are expected to unbind more completely compared to the more strongly bound states, e.g., $\Upsilon(1S)$. At even higher temperatures, more of the weakly bound states are expected to dissolve. In the experiment, this sequential unbinding (also referred to as melting) of quarkonium states is expected to be observed as a sequential suppression of their yields. The suppression of heavy quarkonium states was accordingly proposed as the key signature of the phase transition and its sequential pattern as a probe of the medium temperature [5].

In the early days, most of the attention was devoted to the suppression of charmonium states in collider experiments at super proton synchrotron (SPS) and RHIC. However, even after decades of intense efforts, the experimental observations are not yet completely understood. The suppression of $\psi(1S)$ does not increase from SPS to RHIC, or from RHIC to LHC, even though in each change of accelerator the center-of-mass energy is increased by one order of magnitude. The most accepted explanation for this "unsuppression" is that heavy quarks, evolving independently in the QGP, recombine, forming bound states. This process is called recombination or regeneration [5,6]. It is supposed to take place in the hot plasma and hence to affect mostly the charmonium states produced with transverse momenta typical of the quark-gluon fluid. Indeed, the relative (compared to the scaled pp baseline) reduction of the J/ψ multiplicity measured in AA collisions at low p_T is significantly smaller at LHC energies than at RHIC energies. This is consistent with the regeneration mechanism since the larger charm production cross section at LHC enhances the probability of recombination. The situation changes at high p_T, where the suppression rises as the collision energy increases, revealing that the J/ψ yield is less sensitive to recombination [7–9].

While charmonium states have been extensively studied as QGP probes, bottomonium states have not been explored as much, even though the $b\bar{b}$ family of states provides experimentally more robust and theoretically cleaner probes. Moreover, bottomonium states are regarded as better probes because recombination effects are believed to be much less significant than in the charmonium case. Although the recombination effect is expected to increase for bottomonia from RHIC to LHC energies, it is predicted to remain small [10–16].

From the experimental side, the compact muon solenoid (CMS) detector has excellent capabilities for muon detection

[*]luciano.abreu@ufba.br
[†]navarra@if.usp.br
[‡]mnielsen@if.usp.br

and provides measurements of the Υ family which enable the accurate analysis of bottomonium [17] production. For this reason, the main interest may be shifted to the suppression of bottomonium states at LHC energies. The first indication of Υ suppression in heavy-ion collisions was reported by CMS in 2011 [18]. Later, it was also observed by the STAR Collaboration at RHIC [19]. The $\Upsilon(2S)$ and $\Upsilon(3S)$ resonances in Pb-Pb collisions were seen to be more strongly suppressed than the $\Upsilon(1S)$ (compared with the pp result), showing the expected sequential suppression pattern [17].

The most recent data on prompt J/ψ [20] and Υ [17,21–23] suppression in the most central Pb-Pb collisions at small rapidities and small p_T, show that

$$R_{AA}(J/\psi) \simeq 0.28 \pm 0.03 \tag{1}$$

and

$$R_{AA}(\Upsilon(1S)) \simeq 0.38 \pm 0.05. \tag{2}$$

These factors are very weakly dependent on the collision energy $\sqrt{s_{NN}}$. Although they are close to each other, they may be the result of quite different dynamics.

After the QGP cooling and hadronization, there is a hadron gas (HG) phase. Apart from being a reasonable assumption, the existence of this phase seems to be necessary to correctly reproduce [24] the multiplicities of K^* and ρ measured by the ALICE Collaboration [25–27]. Heavy quarkonium is produced at the beginning of the heavy-ion collision. Then it may be destroyed and regenerated both in the quark gluon plasma and in the subsequent hadron gas. The observed Υ suppression has been explained mostly with models which take into account only what happens during the QGP phase. In this work we address the contribution of the hadron gas phase to the Υ production and absorption.

In the literature, there is a large number of works on quarkonium interactions with light mesons in a hot hadron gas using different approaches (for a short and recent compilation of references on charmonium interactions, see Ref. [28]). Many of these works investigate the J/ψ-light-meson reactions based on effective hadron Lagrangians [28–31]. After a long series of works, different groups found a similar value of the $J/\psi - \pi$ cross section, which is close to the value obtained with QCD sum rules [32]. In Ref. [28], we have used all the known charmonium-light-hadron absorption cross sections (together with the inverse interactions in which charmonium is produced) as input to solve the rate equation which governs the time evolution of J/ψ abundance in a hadron gas. The effective Lagrangian approach will be employed also to the bottomonium in the next sections.

In contrast to the J/ψ case, the number of studies about the Υ interactions with light hadrons is much smaller [33]. In fact, to the best of our knowledge, the paper by Lin and Ko [34] is the only one to give an estimate of the cross sections for scattering of Υ by pions and ρ mesons in a hot hadron gas. In that work, the authors used a hadronic Lagrangian based on the SU(5) flavor symmetry. Including form factors with a cutoff parameter of 1 or 2 GeV at the interaction vertices, they found that the values of $\sigma_{\pi\Upsilon}$ and $\sigma_{\rho\Upsilon}$ are about 8 and 1 mb, respectively. However, their thermal averages at a temperature of 150 MeV are both around only 0.2 mb. The reason for this reduction comes from the momentum average made in the thermal average. The kinematical threshold plays an important role since the sum of the masses of the initial state is $\simeq$9597 MeV and the sum of the masses of the final $B\bar{B}$ state (the lightest one) is $\simeq$10 558. Hence, their difference is $\simeq$960 MeV, which is still much larger than the temperature, $\simeq$150 MeV, and it is responsible for the strong reduction from 8 to 0.2 mb. They then conclude, speculating that the absorption of directly produced Υ by comoving hadrons is unlikely to be important.

In view of the recent theoretical and experimental progress on Υ physics, we believe that it is time to update and extend the calculation of Ref. [34]. In the present work, we will contribute to this subject by extending the analysis performed in Ref. [28] to the bottomonia sector: We investigate the interactions of Υ with the surrounding hadronic medium composed of the lightest pseudoscalar meson (π) and the lightest vector meson (ρ). We calculate the cross sections for processes such as $\bar{B}^{(*)} + B^{(*)} \to \Upsilon + (\pi, \rho)$ scattering and their inverses, within the effective hadron Lagrangian framework. We improve the previous calculation, introducing anomalous interactions. The obtained cross sections are used as input to solve the rate equation which allows us to follow the time evolution of the Υ multiplicity.

The importance of the anomalous vertices has been earlier mentioned in different contexts. For example, in Ref. [30] the J/ψ absorption cross sections by pions and ρ mesons were evaluated for several processes, producing D and D^* mesons in the final state. The authors found that the $J/\psi\pi \to D^*\bar{D}$ cross section obtained with the exchange of a D^* meson in the t channel, which involves the anomalous $D^*D^*\pi$ coupling, was around 80 times bigger than the one obtained with a D meson exchange in the t channel. In Ref. [35], the authors studied the radiative decay modes of the $f_0(980)$ and $a_0(980)$ resonances, finding that the diagrams involving anomalous couplings were quite important for most of the decays. More recently, in Refs. [36,37] it was shown that the inclusion of anomalous interactions produces significant changes in the $X(3872)\pi$ cross section.

As will be seen, the introduction of anomalous interactions leads to a hadronic suppression of Υ which is stronger than expected in Ref. [34].

This work is organized as follows. In Sec. II, we present an overview of the effective Lagrangian formalism and calculate the cross section for Υ production and absorption. The results obtained for the thermally averaged cross sections are exhibited and discussed in Sec. III. After that, Sec. IV is dedicated to the analysis of Υ abundance in heavy-ion collisions. Finally, in Sec. V, we summarize the results and conclusions.

II. INTERACTIONS BETWEEN Υ AND LIGHT MESONS

A. Effective Lagrangian formalism

In the present study, the reactions involving the Υ production and absorption will be analyzed in the effective field theory approach. Accordingly, we follow Refs. [28–30] and employ the couplings between light- and heavy-meson fields

within the framework of an SU(4) effective formalism, in which the vector mesons are identified as the gauge bosons. The procedure to obtain the effective Lagrangian is well explained, e.g., in Refs. [29,30] and the effective Lagrangians for π, ρ, B, and B^* then read

$$\begin{aligned}
\mathcal{L}_{B^*B\pi} &= ig_{B^*B\pi}(B^*_\mu \partial^\mu \pi \bar{B} - B\partial^\mu \pi \bar{B}^*_\mu),\\
\mathcal{L}_{\Upsilon BB} &= ig_{\Upsilon BB}\Upsilon_\mu(\partial^\mu B\bar{B} - B\partial^\mu \bar{B}),\\
\mathcal{L}_{\Upsilon B^*B^*} &= -ig_{\Upsilon B^*B^*}\{\Upsilon^\mu(\partial_\mu B^{*\nu}\bar{B}^*_\nu - B^{*\nu}\partial_\mu \bar{B}^*_\nu)\\
&\quad + (\partial_\mu \Upsilon_\nu B^{*\nu} - \Upsilon_\nu \partial_\mu B^{*\nu})\bar{B}^{*\mu}\\
&\quad + B^{*\mu}(\Upsilon^\nu \partial_\mu \bar{B}^*_\nu - \partial_\mu \Upsilon_\nu \bar{B}^{*\nu})\},\\
\mathcal{L}_{\Upsilon B^*B\pi} &= g_{\Upsilon B^*B\pi}\Upsilon^\mu(B\pi \bar{B}^*_\mu + B^*_\mu \pi \bar{B}),\\
\mathcal{L}_{BB\rho} &= ig_{BB\rho}(B\rho^\mu \partial_\mu \bar{B} - \partial_\mu B\rho^\mu \bar{B}),\\
\mathcal{L}_{B^*B^*\rho} &= ig_{B^*B^*\rho}\{\partial_\mu B^*_\nu \rho^\mu \bar{B}^{*\nu} - B^*_\nu \rho_\mu \partial^\mu \bar{B}^{*\nu}\\
&\quad + (B^{*\nu}\partial_\mu \rho_\nu - \partial_\mu B^*_\nu \rho^\nu)\bar{B}^{*\mu}\\
&\quad + B^{*\mu}(\rho^\nu \partial_\mu \bar{B}^*_\nu - \partial_\mu \rho_\nu \bar{B}^{*\nu})\},\\
\mathcal{L}_{\Upsilon BB\rho} &= -g_{\Upsilon BB\rho}\Upsilon^\mu B\rho_\mu \bar{B},\\
\mathcal{L}_{\Upsilon B^*B^*\rho} &= g_{\Upsilon B^*B^*\rho}\Upsilon_\mu(2B^{*\nu}\rho^\mu \bar{B}^*_\nu - B^{*\nu}\rho_\nu \bar{B}^{*\mu} - B^{*\mu}\rho^\nu \bar{B}^*_\nu).
\end{aligned} \tag{3}$$

We also consider anomalous parity interactions in addition to the interactions given above. The anomalous parity interactions can be described in terms of the gauged Wess-Zumino action [30] and are written as

$$\begin{aligned}
\mathcal{L}_{B^*B^*\pi} &= -g_{B^*B^*\pi}\varepsilon^{\mu\nu\alpha\beta}\partial_\mu B^*_\nu \pi \partial_\alpha \bar{B}^*_\beta,\\
\mathcal{L}_{\Upsilon B^*B} &= -g_{\Upsilon B^*B}\varepsilon^{\mu\nu\alpha\beta}\partial_\mu \Upsilon_\nu(\partial_\alpha B^*_\beta \bar{B} + B\partial_\alpha \bar{B}^*_\beta),\\
\mathcal{L}_{\Upsilon BB\pi} &= -ig_{\Upsilon BB\pi}\varepsilon^{\mu\nu\alpha\beta}\Upsilon_\mu \partial_\nu B\partial_\alpha \pi \partial_\beta \bar{B},\\
\mathcal{L}_{\Upsilon B^*B^*\pi} &= -ig_{\Upsilon B^*B^*\pi}\varepsilon^{\mu\nu\alpha\beta}\Upsilon_\mu B^*_\nu \partial_\alpha \pi \bar{B}^*_\beta\\
&\quad - ih_{\Upsilon B^*B^*\pi}\varepsilon^{\mu\nu\alpha\beta}\partial_\mu \psi_\nu B^*_\alpha \pi \bar{B}^*_\beta,\\
\mathcal{L}_{B^*B\rho} &= -g_{B^*B\rho}\varepsilon^{\mu\nu\alpha\beta}(B\partial_\mu \rho_\nu \partial_\alpha \bar{B}^*_\beta + \partial_\mu B^*_\nu \partial_\alpha \rho_\beta \bar{B}),\\
\mathcal{L}_{\Upsilon B^*B\rho} &= ig_{\Upsilon B^*B\rho}\varepsilon^{\mu\nu\alpha\beta}\Upsilon_\mu(\partial_\nu B\rho_\alpha \bar{B}^*_\beta + B^*_\nu \rho_\alpha \partial_\beta \bar{B})\\
&\quad - ih_{\Upsilon B^*B\rho}\varepsilon^{\mu\nu\alpha\beta}\Upsilon_\mu(B\rho_\nu \partial_\alpha \bar{B}^*_\beta - \partial_\nu B^*_\alpha \rho_\beta \bar{B}),
\end{aligned} \tag{4}$$

with $\varepsilon_{0123} = +1$.

The effective Lagrangians given in Eqs. (3) and (4) allow us to study the following $\varphi\Upsilon$ absorption processes:

$$\begin{aligned}
&(1)\ \varphi\Upsilon \to \bar{B}B,\\
&(2)\ \varphi\Upsilon \to \bar{B}^*B,\\
&(3)\ \varphi\Upsilon \to \bar{B}^*B^*,
\end{aligned} \tag{5}$$

where in the initial states φ stand for pions and ρ mesons. The process $\varphi\Upsilon \to \bar{B}B^*$ has the same cross section as the process (2) in Eq. (5). In the present approach, the diagrams considered to compute the amplitudes of the processes above are of two types: one-meson exchange and contact graphs. They are shown in Figs. 1 and 2 for those with pions and ρ, respectively.

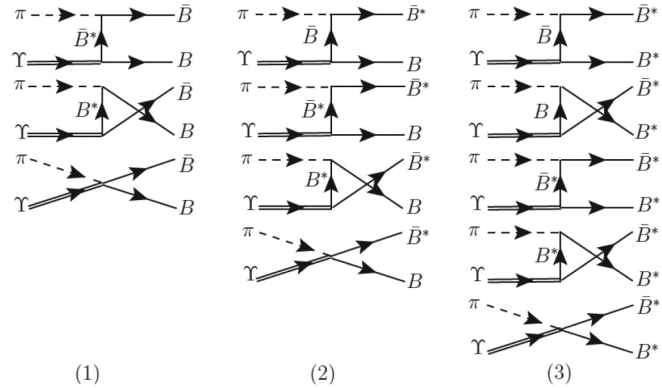

FIG. 1. Diagrams contributing to the processes: (1) $\pi\Upsilon \to \bar{B}B$, (2) $\pi\Upsilon \to \bar{B}^*B$, and (3) $\pi\Upsilon \to \bar{B}^*B^*$.

We define the invariant amplitudes for the processes (1)–(3) in Eq. (5) involving $\varphi = \pi$ meson as

$$\begin{aligned}
\mathcal{M}^{(\pi)}_1 &= \sum_i \mathcal{M}^{(\pi)\mu}_{1i}\epsilon_\mu(p_1),\\
\mathcal{M}^{(\pi)}_2 &= \sum_i \mathcal{M}^{(\pi)\mu\nu}_{2i}\epsilon_\mu(p_1)\epsilon^*_\nu(p_3).\\
\mathcal{M}^{(\pi)}_3 &= \sum_i \mathcal{M}^{(\pi)\mu\nu\lambda}_{3i}\epsilon_\mu(p_1)\epsilon^*_\nu(p_3)\epsilon^*_\lambda(p_4),
\end{aligned} \tag{6}$$

while for the ones involving $\varphi = \rho$ meson we have

$$\begin{aligned}
\mathcal{M}^{(\rho)}_1 &= \sum_i \mathcal{M}^{(\rho)\mu\nu}_{1i}\epsilon_\mu(p_1)\epsilon_\nu(p_2),\\
\mathcal{M}^{(\rho)}_2 &= \sum_i \mathcal{M}^{(\rho)\mu\nu\lambda}_{2i}\epsilon_\mu(p_1)\epsilon_\nu(p_2)\epsilon^*_\lambda(p_3).\\
\mathcal{M}^{(\rho)}_3 &= \sum_i \mathcal{M}^{(\rho)\mu\nu\lambda\delta}_{3i}\epsilon_\mu(p_1)\epsilon_\nu(p_2)\epsilon^*_\lambda(p_3)\epsilon^*_\delta(p_4).
\end{aligned} \tag{7}$$

In the above equations, the sum over i represents the sum over all diagrams contributing to the respective amplitude; p_j denotes the momentum of particle j, with particles 1 and 2 standing for initial-state mesons and particles 3 and 4 for final-state mesons; $\epsilon_\mu(p_j)$ is the polarization vector related to the respective vector particle j. The specific expressions of

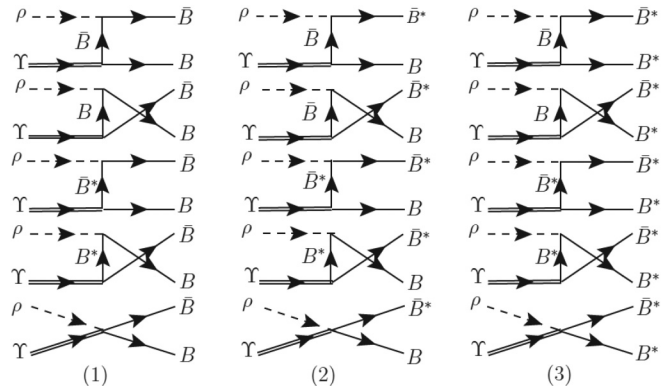

FIG. 2. Diagrams contributing to the processes: (1) $\rho\Upsilon \to \bar{B}B$, (2) $\rho\Upsilon \to \bar{B}^*B$, and (3) $\rho\Upsilon \to \bar{B}^*B^*$.

TABLE I. Values of coupling constants [30,34].

Coupling constant	Value
$g_{B^*B\pi}$	24.9
$g_{\Upsilon BB}$	13.3
$g_{\Upsilon B^*B^*}$	13.3
$g_{BB\rho}$	2.52
$g_{B^*B^*\rho}$	2.52
$g_{\Upsilon B^*B\pi}$	165.6
$g_{\Upsilon BB\rho}$	67.03
$g_{\Upsilon B^*B^*\rho}$	33.5
$g_{B^*B^*\pi}$	9.39 GeV^{-1}
$g_{\Upsilon B^*B}$	2.51 GeV^{-1}
$g_{B^*B\rho}$	1.84 GeV^{-1}
$g_{\Upsilon BB\pi}$	44.8 GeV^{-3}
$g_{\Upsilon B^*B^*\pi}$	31.25 GeV^{-1}
$h_{\Upsilon B^*B^*\pi}$	31.25 GeV^{-1}
$g_{\Upsilon B^*B\rho}$	6.33 GeV^{-1}
$h_{\Upsilon B^*B\rho}$	6.33 GeV^{-1}

amplitudes $\mathcal{M}_i^{(\pi)}$ and $\mathcal{M}_i^{(\rho)}$ in the present case are analogous to the ones given in Ref. [30] involving $\varphi J/\psi \to D^{(*)}\bar{D}^{(*)}$. So, we will not reproduce here the explicit expressions of the invariant amplitudes. These expressions can be found in Ref. [30], taking into account the replacement of masses and coupling constants labeled with charmed mesons and J/ψ by similar quantities labeled with bottomed mesons and Υ, respectively.

The isospin-spin-averaged cross section for the processes in Eq. (5) is defined in the center-of-mass (c.m.) frame as

$$\sigma_r^{(\varphi)}(s) = \frac{1}{64\pi^2 s}\frac{|\vec{p}_f|}{|\vec{p}_i|}\int d\Omega \overline{\sum_{S,I}}\left|\mathcal{M}_r^{(\varphi)}(s,\theta)\right|^2, \tag{8}$$

where $r = 1, 2, 3$ labels $\varphi - \Upsilon$ absorption processes according to Eqs. (6) and (7); $\sqrt{s}$ is the c.m. energy; $|\vec{p}_i|$ and $|\vec{p}_f|$ denote the three-momenta of initial and final particles in the c.m. frame, respectively; the symbol $\overline{\sum_{S,I}}$ represents the sum over the spins and isospins of the particles in the initial and final states, weighted by the isospin and spin degeneracy factors of the two particles forming the initial state for the reaction r, i.e.,

$$\overline{\sum_{S,I}}|\mathcal{M}_r|^2 = \frac{1}{g_1 g_2}\sum_{S,I}|\mathcal{M}_r|^2, \tag{9}$$

with $g_1 = (2I_{1i,r}+1)(2S_{1i,r}+1)$, $g_2 = (2I_{2i,r}+1)(2S_{2i,r}+1)$ being the degeneracy factors of the initial particles 1 and 2.

We have employed in the computations of the present work the isospin-averaged masses: $m_\pi = 137.3$ MeV, $m_\rho = 775.2$ MeV, $m_B = 5279.4$ MeV, $m_{B^*} = 5324.7$ MeV, and $m_\Upsilon = 9460.3$ MeV. The values of coupling constants appearing in the expressions of the amplitudes $\mathcal{M}^{(\pi)}$ and $\mathcal{M}^{(\rho)}$ are given in Table I [30,34].

We have also included form factors in the vertices when evaluating the cross sections, defined as [38–40]

$$F_3 = \left[\frac{n\Lambda^4}{n\Lambda^4 + \left(p^2 - m_{ex}^2\right)^2}\right]^n,$$
$$F_4 = \left\{\frac{n\Lambda^4}{n\Lambda^4 + [(p_1+p_2)^2 - (m_3+m_4)^2]}\right\}^n, \tag{10}$$

where F_3 and F_4 are the form factors for the three-point and four-point vertices, respectively; p is the four-momentum of the exchanged particle of mass m_{ex} for a vertex involving a t- or u-channel meson exchange; and m_3 and m_4 are the final-state meson masses. Unless differently stated, the cutoff Λ and n parameters are chosen to be $\Lambda = 5.0$ GeV and $n \to \infty$ for all vertices, which gives Gaussian form factors with width 25.0 GeV^2. This choice of Λ is "natural" because it is of the order of magnitude of the b quark mass (and also of the B meson mass) and also because it leads to values of the cross sections which are close to those found in Ref. [34]. In that work, the authors had to choose a value for their cutoff parameter, which was taken to be 1 or 2 GeV, and they had no deep justification for their choice.

In some specific cases, form factors can be calculated with QCD sum rules [41]. For all others, the form is arbitrary. This is a known problem when working with form factors. The same is true for the procedure used to fix the cutoff values. In the literature on light hadron interactions, the cutoff can be fixed so as to reproduce some experimental observable. In general, one uses monopole (m), dipole (d), or exponential (e) forms for the form factor. From experience, one learns that the cutoff value is of the order of $m_{\text{min}} < \Lambda < m_{\text{max}}$, where m_{min} (m_{max}) is the mass of the lightest (heaviest) particle entering or exiting the vertex. Morever, concerning the different parametrizations, we learn that $\Lambda^{(m)} \simeq 0.62\,\Lambda^{(d)} \simeq 0.78\,\Lambda^{(e)}$. The forms used in the equations above have the advantage of dealing with invariant quantities (products of four-momenta). Other forms, used, e.g., in Refs. [30,34,38], use three-momenta. We use these notions and follow closely Ref. [39] to define our parameters.

B. Υ production and absorption cross sections

In the top panel of Fig. 3, the $\pi\Upsilon$ absorption cross sections for the $\pi\Upsilon \to \bar{B}B$, $\bar{B}^*B$, and $\bar{B}^*B^*$ reactions are plotted as a function of the c.m. energy $\sqrt{s}$. We see that the cross sections can be considered to be approximately of the same order of magnitude in the range 10.6 GeV $\leqslant \sqrt{s} \leqslant$ 11.8 GeV, differing by about a factor 1.5–3. The magnitude of the reaction $\pi\Upsilon \to \bar{B}^*B$ is in agreement with previous calculations reported in Ref. [34], which is based in SU(5) symmetry, using different form factors, cutoffs, and coupling constants and without anomalous terms. The authors of Ref. [34] did not include some of the processes with final states $\bar{B}B$ and $\bar{B}^*B^*$.

The cross sections of the processes $\rho\Upsilon \to \bar{B}B$, $\bar{B}^*B$, and $\bar{B}^*B^*$ are plotted as a function of $\sqrt{s}$ on the bottom panel of Fig. 3. In this case, the cross section for $\rho\Upsilon \to \bar{B}^*B^*$ is larger than the others by about one order of magnitude. As expected, the $\rho - \Upsilon$ reactions have smaller cross sections than those initiated by pions. The findings above are also in

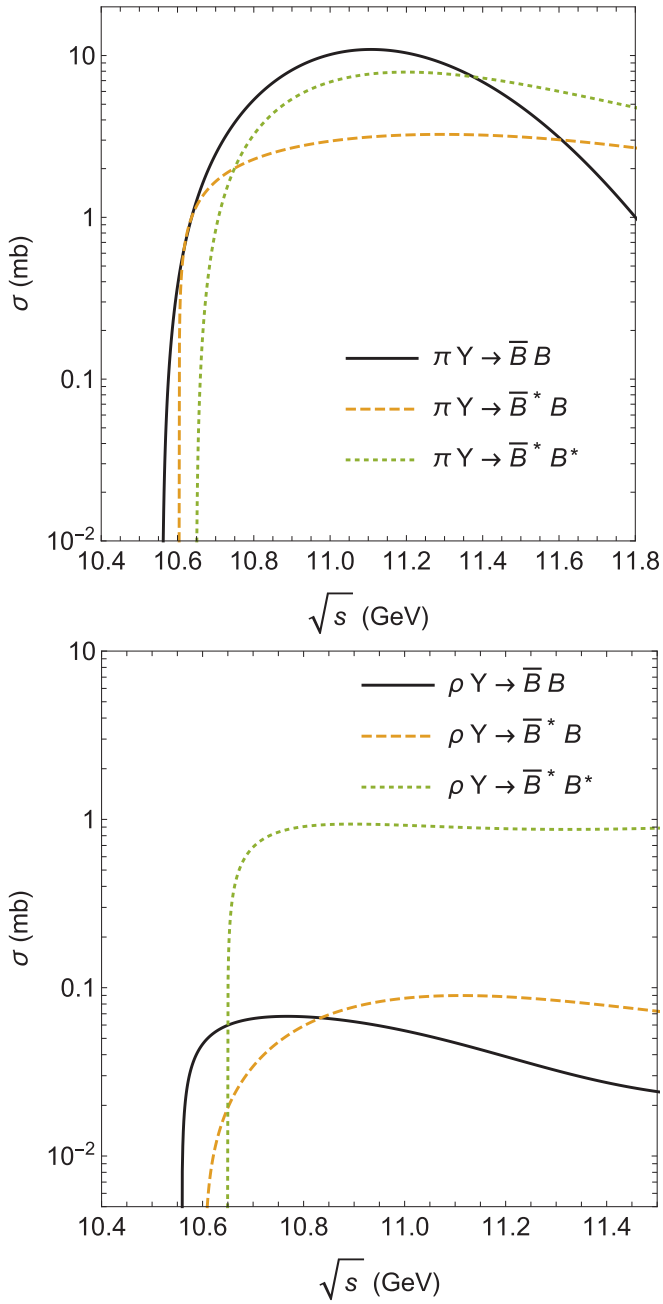

FIG. 3. ϒ absorption cross sections in different processes as a function of the c.m. energy $\sqrt{s}$. Top panel: $\pi\Upsilon$ in the initial state. Bottom panel: $\rho\Upsilon$ in the initial state. Solid, dashed, and dotted lines represent the $\pi(\rho)\Upsilon \to \bar{B}B$, $\pi(\rho)\Upsilon \to \bar{B}^*B$, and $\pi(\rho)\Upsilon \to \bar{B}^*B^*$ reactions, respectively.

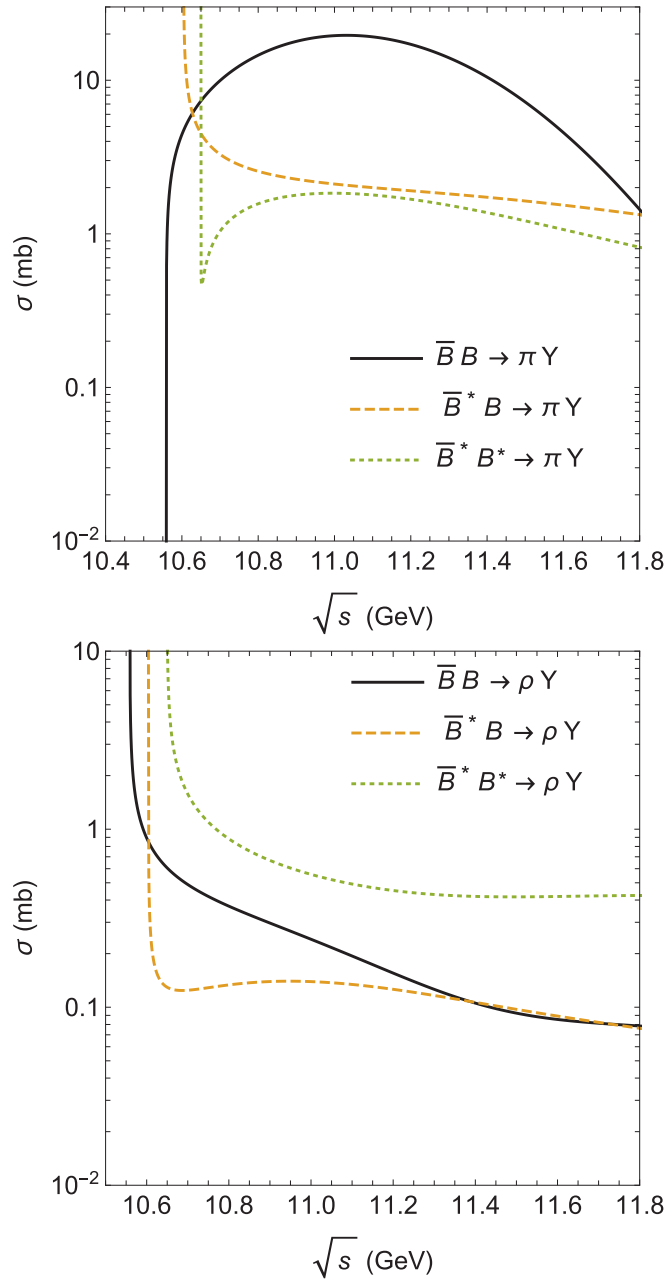

FIG. 4. ϒ production cross sections in different processes as a function of the c.m. energy $\sqrt{s}$. Top panel: $\pi\Upsilon$ in the final state. Bottom panel: $\rho\Upsilon$ in the final state. Solid, dashed, and dotted lines represent the $\bar{B}B \to \pi(\rho)\Upsilon$, $\bar{B}^*B \to \pi(\rho)\Upsilon$, and $\bar{B}^*B^* \to \pi(\rho)\Upsilon$ reactions, respectively.

relative agreement with the previous calculations reported in Ref. [34], although only the processes which end with $\bar{B}B$ and $\bar{B}^*B^*$ have been considered in Ref. [34]. Again, we believe that the differences are due to different choices in the form factors and cutoff values, and the absence of anomalous parity interactions.

For completeness, we now calculate the cross sections of the inverse processes, which can be obtained from the direct processes through the use of detailed balance (see, for example, Eq. (48) of the last article of Ref. [29]). In the top (bottom) panel of Fig. 4, the $\pi(\rho)\Upsilon$ production cross sections for the $\bar{B}B \to \pi(\rho)\Upsilon$, $\bar{B}B^* \to \pi(\rho)\Upsilon$, and $\bar{B}^*B^* \to \pi(\rho)\Upsilon$ reactions are plotted as a function of the c.m. energy $\sqrt{s}$.

From these figures, we can see that (i) processes which start or end with $\pi\Upsilon$ have larger cross sections, and (ii) excluding the low-energy region (which will be much less relevant for phenomenology), the ϒ production and absorption cross sections are close to each other in almost all channels. Therefore,

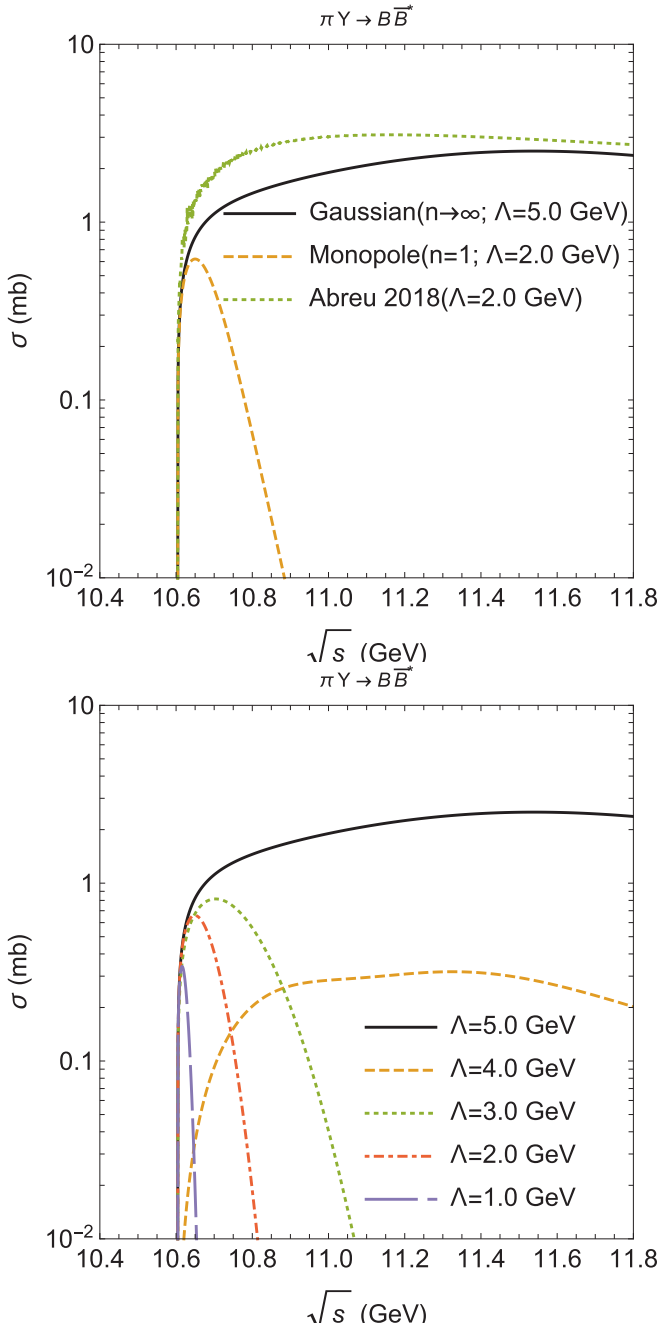

FIG. 5. Top panel: Υ production cross sections for different choices of the form factor. Bottom panel: Υ production cross sections for a Gaussian form factor with different choices of the cutoff.

taking into account that the Υ absorption and production cross sections have comparable magnitudes, the computation of thermally averaged cross sections is an essential step to determine the final abundance of Υ's. This will be done in next section.

Before closing this section, we present in Fig. 5 the dependence of our results on the form of the form factor [Fig. 5(a)] and on the choice of the cutoff [Fig. 5(b)]. As can be seen, both the form of the form factor and the cutoff value have significant impacts on the final cross section.

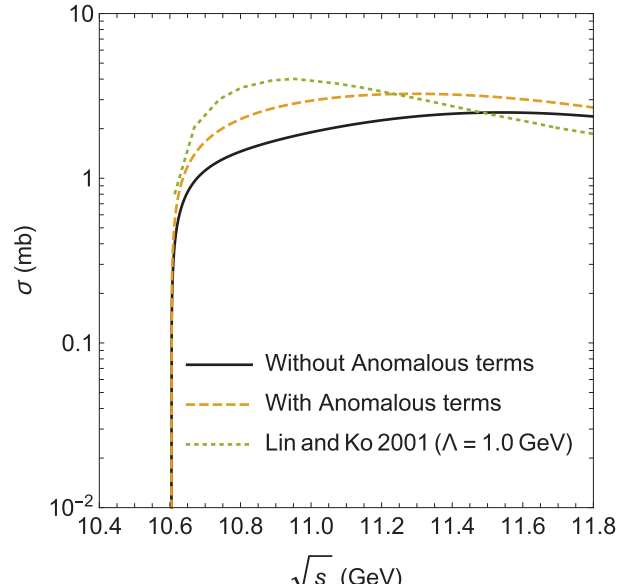

FIG. 6. Υ absorption cross section computed with our model with (dashed line) and without (solid line) anomalous interactions. Here we consider only the channel $\Upsilon\pi \to \bar{B}^*B$. We also show the result obtained in Ref. [34] (dotted line).

In Fig. 6, we show a comparison between our results for the process $\Upsilon\pi \to \bar{B}^*B$ and those obtained in Ref. [34]. The actual values of the cross sections depend, among other things, on the form factors, on the cutoff choices, and on the adopted values for coupling constants. Nevertheless, we can clearly see that including the anomalous terms increases the cross section. Our values are slightly larger than those found in Ref. [34] but this difference is important and will be amplified in the calculation of the Υ abundance.

III. THERMALLY AVERAGED CROSS SECTIONS

The thermally averaged cross section for a given process $ab \to cd$ is defined as [36,42–44]

$$\langle \sigma_{ab\to cd} v_{ab} \rangle = \frac{\int d^3\mathbf{p}_a d^3\mathbf{p}_b f_a(\mathbf{p}_a) f_b(\mathbf{p}_b) \sigma_{ab\to cd}\ v_{ab}}{\int d^3\mathbf{p}_a d^3\mathbf{p}_b f_a(\mathbf{p}_a) f_b(\mathbf{p}_b)}$$
$$= \frac{1}{4\alpha_a^2 K_2(\alpha_a)\alpha_b^2 K_2(\alpha_b)} \times \int_{z_0}^{\infty} dz K_1(z)\ \sigma(s = z^2T^2) \times [z^2 - (\alpha_a + \alpha_b)^2][z^2 - (\alpha_a - \alpha_b)^2], \quad (11)$$

where v_{ab} represents the relative velocity of the two initial interacting particles a and b; the function $f_i(\mathbf{p}_i)$ is the Bose-Einstein distribution (of particles of species i), which depends on the temperature T; $\alpha_i = m_i/T$, $z_0 = \max(\alpha_a + \alpha_b, \alpha_c + \alpha_d)$, and K_1 and K_2 are the modified Bessel functions of the second kind.

In Fig. 7, we plot the thermally averaged cross sections for $\pi\Upsilon$ absorption (upper panel) and production (lower panel) via

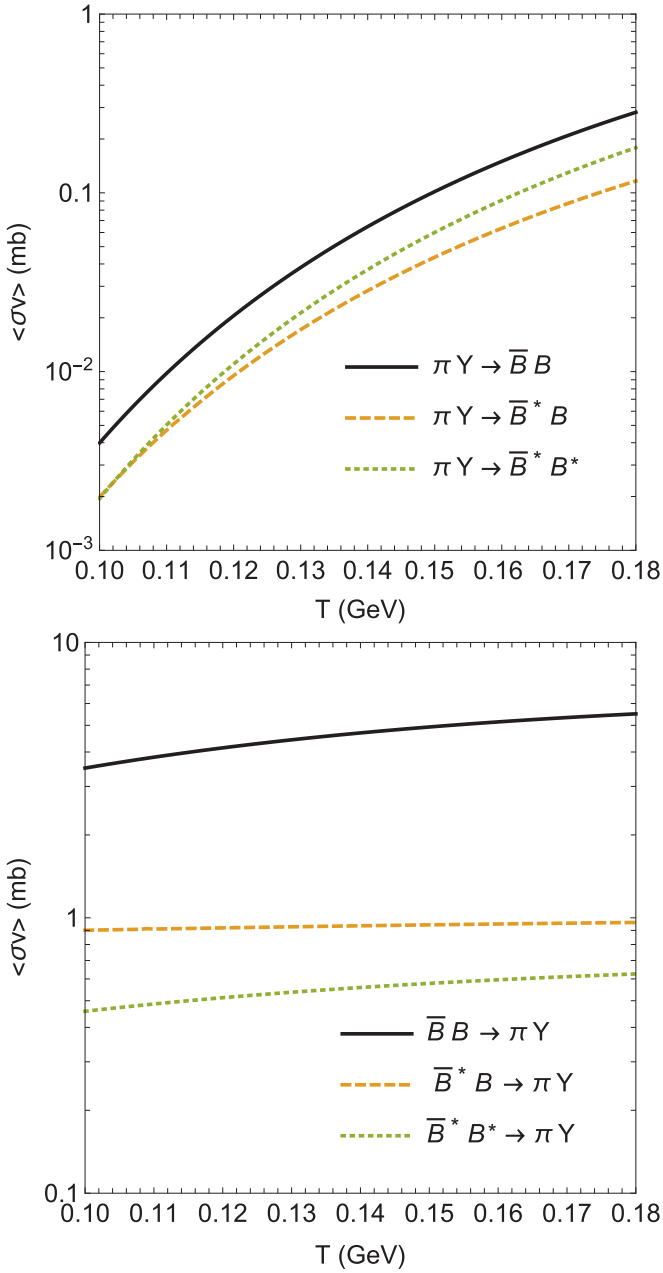

FIG. 7. Thermally averaged cross sections for $\pi\Upsilon$ absorption and production as a function of the temperature. Top panel: $\pi\Upsilon$ in the initial state. Bottom panel: $\pi\Upsilon$ in the final state. Solid, dashed, and dotted lines represent the reactions with $\bar{B}B$, $\bar{B}^*B$, and $\bar{B}^*B^*$, respectively, in final or initial states.

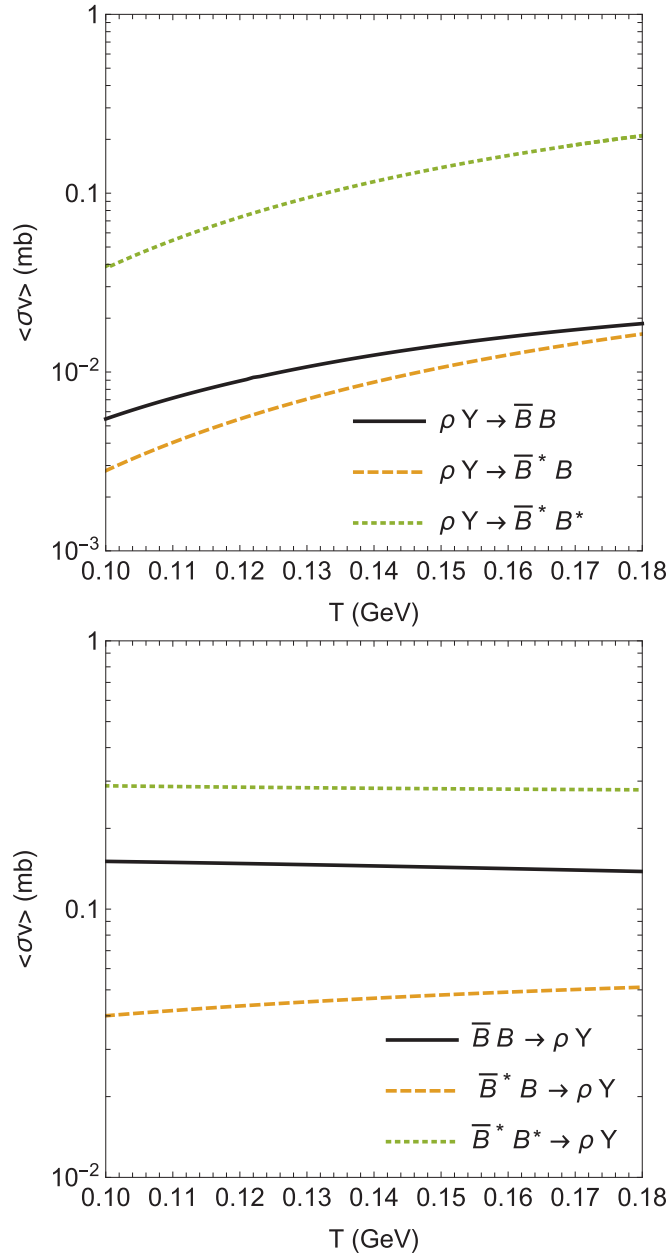

FIG. 8. Thermally averaged cross sections for $\rho\Upsilon$ absorption and production as a function of the temperature. Top panel: $\rho\Upsilon$ in the initial state. Bottom panel: $\rho\Upsilon$ in the final state. Solid, dashed, and dotted lines represent the reactions with $\bar{B}B$, $\bar{B}^*B$, and $\bar{B}^*B^*$, respectively, in final or initial states.

the processes discussed in previous section. In Fig. 8, we plot the thermally averaged cross sections for the $\rho\Upsilon$ absorption and production. As can be seen, in general the production reactions have larger cross sections than the corresponding inverse reactions.

The range of temperatures which is relevant for our discussion corresponds to a very narrow range of energies $\sqrt{s}$, not far from the reaction thresholds. Figures 7 and 8 preserve the relative importance of the channels and they reproduce what is observed in Figs. 3 and 4. In other words, the thermal averaging does not change the relative ordering of the cross sections.

IV. TIME EVOLUTION OF THE ϒ ABUNDANCE

The present study will be completed by addressing the time evolution of the Υ abundance in hadronic matter, using the thermally averaged cross sections estimated in the previous section. We shall make use of the evolution equation for the abundances of particles included in processes discussed above. The momentum-integrated evolution equation has the

TABLE II. Parameters used in the parametrization of the hydrodynamical expansion, given by Eqs. (14).

	$\sqrt{s_{NN}}$ (TeV)	v_C (c)	a_C (c^2/fm)	R_C (fm)	τ_C (fm/c)	τ_H (fm/c)	τ_F (fm/c)	γ_b	N_b	N_Υ
RHIC	0.2	0.4	0.02	8	5	7.5	17.3	2.2×10^6	0.03	1.7×10^{-6}
LHC-I	5	0.5	0.03	11	7.1	10.2	21.5	3.3×10^7	0.71	0.001
LHC-II	5	0.5	0.09	11	7.1	10.2	21.5	1.4×10^9	0.71	0.002

form [36,43–48]:

$$\begin{aligned}\frac{dN_\Upsilon(\tau)}{d\tau} = \sum_{\varphi=\pi,\rho} [&\langle\sigma_{\bar{B}B\to\varphi\Upsilon} v_{\bar{B}B}\rangle n_{\bar{B}}(\tau) N_B(\tau) \\ &- \langle\sigma_{\varphi\Upsilon\to\bar{B}B} v_{\varphi\Upsilon}\rangle n_\varphi(\tau) N_\Upsilon(\tau) \\ &+ \langle\sigma_{\bar{B}^*B^*\to\varphi\Upsilon} v_{\bar{B}^*B^*}\rangle n_{\bar{B}^*}(\tau) N_{B^*}(\tau) \\ &- \langle\sigma_{\varphi\Upsilon\to\bar{B}^*B^*} v_{\varphi\Upsilon}\rangle n_\varphi(\tau) N_\Upsilon(\tau) \\ &+ \langle\sigma_{\bar{B}^*B\to\varphi\Upsilon} v_{\bar{B}^*B}\rangle n_{\bar{B}^*}(\tau) N_B(\tau) \\ &- \langle\sigma_{\varphi\Upsilon\to\bar{B}^*B} v_{\varphi\Upsilon}\rangle n_\varphi(\tau) N_\Upsilon(\tau) \\ &+ \langle\sigma_{\bar{B}B^*\to\varphi\Upsilon} v_{\bar{B}B^*}\rangle n_{\bar{B}}(\tau) N_{B^*}(\tau) \\ &- \langle\sigma_{\varphi\Upsilon\to\bar{B}B^*} v_{\varphi\Upsilon}\rangle n_\varphi(\tau) N_\Upsilon(\tau)], \end{aligned} \tag{12}$$

where $n_i(\tau)$ are $N_i(\tau)$ denote the density and the abundances of π, ρ and bottom mesons in hadronic matter at proper time τ. From Eq. (12), we notice that the Υ abundance at a proper time τ depends on the $\varphi\Upsilon$ dissociation rate as well as on the $\varphi\Upsilon$ production rate. We will assume that π, ρ, B, and B^* are in equilibrium. Therefore, the density $n_i(\tau)$ can be written as [36,43–46]

$$n_i(\tau) \approx \frac{1}{2\pi^2}\gamma_i g_i m_i^2 T(\tau) K_2\left(\frac{m_i}{T(\tau)}\right), \tag{13}$$

where γ_i and g_i are the fugacity factor and the degeneracy factor of the relevant particle, respectively. The multiplicity $N_i(\tau)$ is obtained by multiplying the density $n_i(\tau)$ by the volume $V(\tau)$. The time dependence is introduced through the temperature, $T(\tau)$, and volume, $V(\tau)$, profiles, appropriate to model the dynamics of relativistic heavy-ion collisions after the end of the quark-gluon plasma phase. The hydrodynamical expansion and cooling of the hadron gas are described as in Refs. [36,43–48], which are based on the boost-invariant Bjorken picture with an accelerated transverse expansion:

$$\begin{aligned} T(\tau) &= T_C - (T_H - T_F)\left(\frac{\tau - \tau_H}{\tau_F - \tau_H}\right)^{\frac{4}{5}}, \\ V(\tau) &= \pi\left[R_C + v_C(\tau - \tau_C) + \frac{a_C}{2}(\tau - \tau_C)^2\right]^2 \tau\, c, \end{aligned} \tag{14}$$

where R_C and τ_C denote the final transverse and longitudinal sizes of the quark-gluon plasma; v_C and a_C are its transverse flow velocity and transverse acceleration at τ_C; $T_C = 175$ MeV is the critical temperature for the quark-gluon plasma to hadronic matter transition; $T_H = T_C = 175$ MeV is the temperature of the hadronic matter at the end of the mixed phase, occurring at the time τ_H; and the freeze-out temperature, $T_F = 125$ MeV, leads to a freeze-out time τ_F. These numbers come from the model of the expansion of the medium used in Refs. [36,43–46].

In the present approach, we assume that the total number of bottom quarks, N_b, in bottom hadrons is conserved during the processes. This number can be calculated with perturbative QCD and yields the initial bottom quark fugacity factor γ_b in Eq. (13) [36,43–46]. We note that the conservation of the number of bottom quarks, i.e.,

$$n_b(\tau) \times V(\tau) = N_b = \text{const.} \tag{15}$$

implies that the bottom fugacity γ_b is time dependent. Inserting Eq. (13) into the above expression, we obtain an equation for $\gamma_b(\tau)$ and its solution is used in Eq. (12). The total number of pions and ρ mesons at freeze-out was taken from Refs. [36,47,48]. Since the kinetic freeze-out temperature used here is much lower than the chemical freeze-out temperature, we assume that the π's and ρ's may be out of chemical equilibrium in the later part of the hadronic evolution and have time-dependent fugacities. These fugacities can be calculated in the same way as $\gamma_b(\tau)$.

The evolution of Υ multiplicity is analyzed in two scenarios: with the hadron gas formed in central Au-Au collisions at $\sqrt{s_{NN}} = 200$ GeV at RHIC and central Pb-Pb collisions at $\sqrt{s_{NN}} = 5$ TeV at the LHC. The parameters which we need as input in Eqs. (14) are listed in Ref. [45] and are reproduced in Table II for convenience. Notice that the estimate of the Υ yield at the end of the mixed phase, given in the last column of Table II, is done in the context of the statistical model, in which hadrons are in thermal and chemical equilibrium when they are produced. Therefore, at RHIC the Υ multiplicity at τ_H is

$$\begin{aligned} N_\Upsilon &\approx \frac{1}{2\pi^2}\gamma_b^2 g_\Upsilon m_\Upsilon^2 T_H K_2\left(\frac{m_\Upsilon}{T_H}\right) V(\tau_H) \\ &\approx 1.7 \times 10^{-6}. \end{aligned} \tag{16}$$

A similar calculation for the case of LHC gives $N_\Upsilon \approx 0.001$.

The time evolution of the Υ abundance is plotted in Fig. 9 as a function of the proper time, for the two types of collisions discussed above: at RHIC (on the upper panel) and at the LHC (on the lower panel) with the parameter set LHC-I. In the panels, each band is defined by an upper line obtained with $\Lambda = 3$ GeV and a lower line obtained with $\Lambda = 5$ GeV. The area of the band corresponds to lines obtained with intermediate values of Λ. Note that since the hadronic stage at LHC is a bit longer compared to that at RHIC, more bottomonium states are lost in the hadronic medium at LHC. Moreover, we can see how important the anomalous interactions are. In both panels, when we include them, the upper bands move to the lower bands and the suppression increases significantly.

As can be noticed from Eq. (12), the evolution of the Υ multiplicity depends on the production and absorption cross sections and also on the abundances of the other mesons.

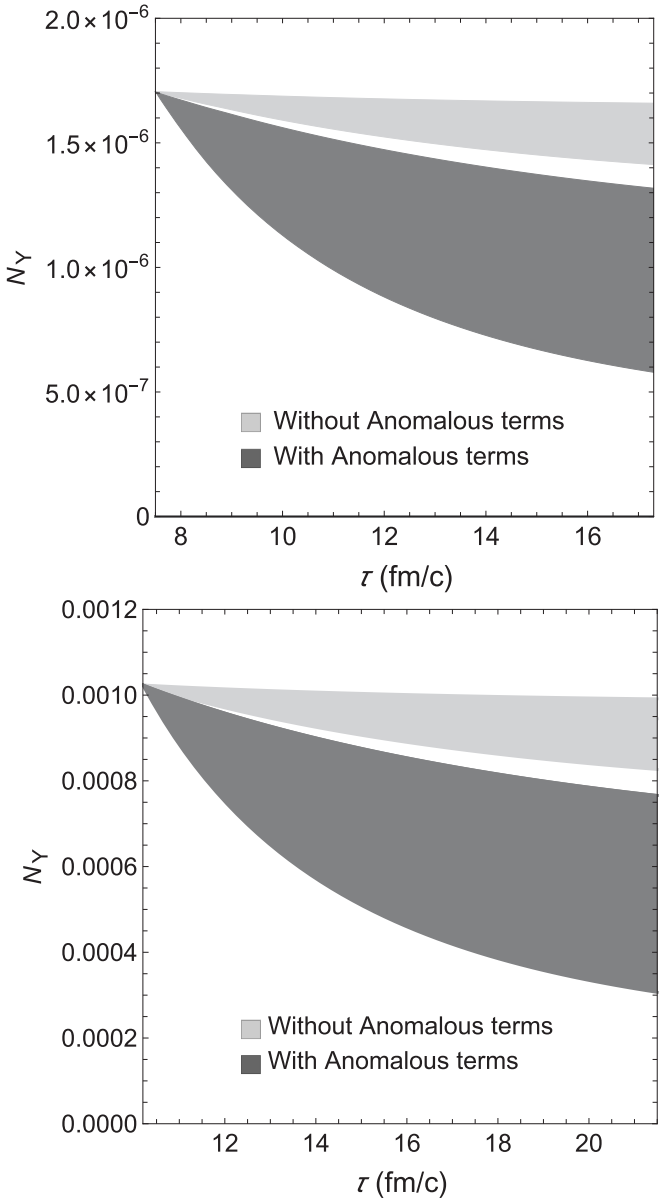

FIG. 9. Top: Time evolution of ϒ abundance as a function of the proper time in central Au-Au collisions at $\sqrt{s_{NN}} = 200$ GeV. Upper and lower limits of the bands are obtained with Λ equal to 3 and 5 GeV respectively. Upper (lower) band is calculated without (with) the anomalous interactions. Bottom: the same as on the top for LHC conditions (parameter set LHC-I).

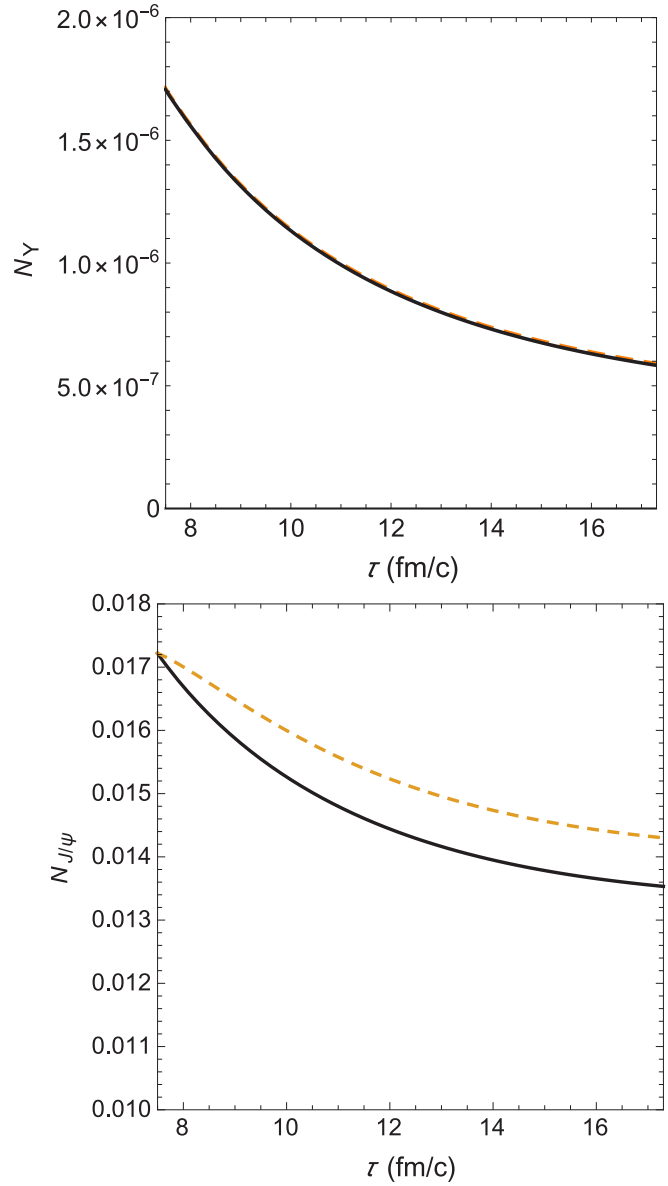

FIG. 10. Top: Time evolution of ϒ abundance as a function of the proper time in central Au-Au collisions at $\sqrt{s_{NN}} = 200$ GeV. Solid line: solution of Eq. (12) only with the absorption terms. Dashed line: solution of Eq. (12) including the regeneration terms. The cutoff Λ was fixed at 5 GeV. Bottom: the same as on the top for the J/ψ.

Although the production cross sections are greater than the absorption ones, which would enhance the ϒ yield, the relative meson multiplicities lead to its reduction, since there are much more light mesons (especially pions) in the hadron gas to collide and destroy the bottomonium states than $B^{(*)}$'s and $\bar{B}^{(*)}$'s to interact and "regenerate" them. In fact, the bottomonium regeneration is numerically insignificant whereas charmonium regeneration in a hot hadron gas is relatively important. This is illustrated in the upper panel of Fig. 10, where we compare the solution of the complete (total) Eq. (12) with the solution obtained keeping only the absorption (loss) terms and disregarding the regeneration (gain) terms. In the lower panel, we show the corresponding results for the charmonium. The difference between the two panels suggests that in the case of charmonium regeneration is important and reduces the net J/ψ suppression whereas in the case of bottomonium it does not make any difference.

In Ref. [49], it has been pointed out that Eq. (12) is correct in the grand canonical case. However, when the average number of B mesons in an event is much lower than 1, the bottom-flavor conservation in each event needs to be implemented exactly and the rate equation is different. In this case, the ϒ abundance could in principle be very different. We can investigate this "canonical suppression" effect substituting

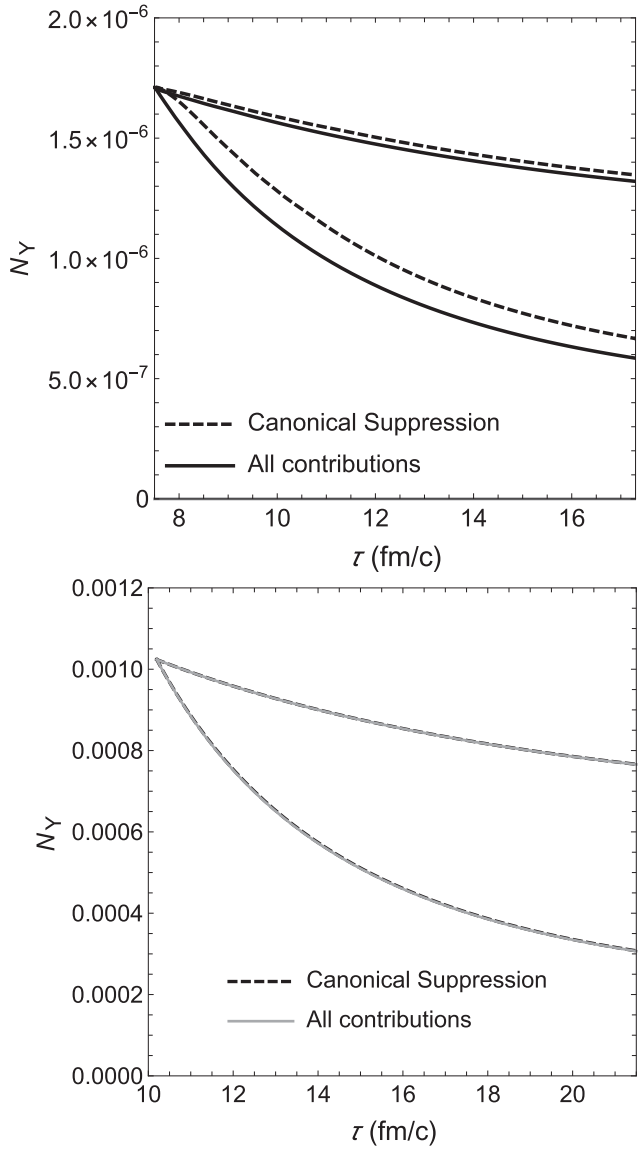

FIG. 11. Top: Time evolution of Υ abundance as a function of the proper time in central Au-Au collisions at $\sqrt{s_{NN}} = 200$ GeV. The dashed lines define the boundaries of the area which contains the solutions of Eq. (12) for different values of Λ. The solid lines define the boundaries of the area which contains the solutions of Eq. (9) of Ref. [49] for different values of Λ. Bottom: the same as on the top for the LHC conditions.

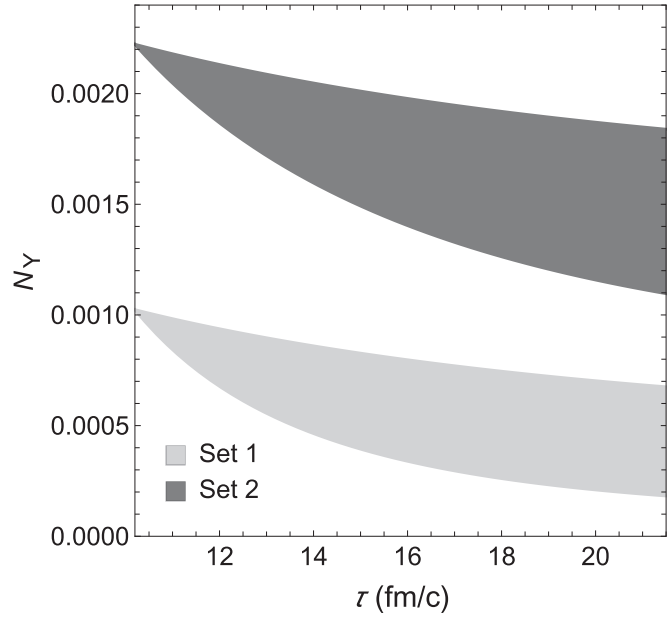

FIG. 12. Time evolution of Υ abundance for two parameter choices. Upper band: LHC-II (with $T_C = 156$ MeV). Lower band: LHC-I (with $T_C = 175$ MeV).

Eq. (12) by the modified rate equation given by Eq. (9) of Ref. [49]. In Fig. 11, we compare the results obtained with the two different rate equations. In each panel, the prediction of the canonical suppression is the area spanned by the two dashed lines to be compared with area spanned by the solid lines obtained with Eq. (12). As expected, the difference between them is bigger at the RHIC lower energies (upper panel) and negligible at higher LHC energies (lower panel).

So far, all the results were obtained with the parameter sets labeled RHIC and LHC-I in Table II. In order to see how much our conclusions on Υ suppression depend on the details of the fluid expansion, we have chosen a second parameter set for the LHC collisions (called LHC-II in Table II). In this set, $T_C = T_H = 156$ MeV and $T_F = 115$ MeV. With this choice other numbers must change so as to reproduce the input information contained in Ref. [45]. As a consequence, the initial Υ abundance is different. This is not a problem here since we are mostly interested in observing how these changes will affect the Υ suppression. The results are shown in Fig. 12. Whereas with LHC-I there is a suppression by a factor up to 3, with LHC-II the strongest suppression is only by a factor 2.

The results shown in Fig. 9 suggest that the reduction of the Υ yield in the hadron gas phase can be sizable and grows slowly with the collision energy. To a large extent, this behavior is a consequence of the anomalous interactions. It is interesting to observe that for certain cut-off choices the Υ suppression is quite similar to the J/ψ suppression found in Ref. [28]. Unfortunately, due to the very strong cutoff dependence of the results (illustrated by the bands), it is not possible to be precise. Moreover, there are other sources of uncertainty. First, the interactions in the reactions are naturally dependent on the effective formalism considered, which determines the magnitudes of the cross sections. A change in the magnitude of the production reactions will modify those of the absorption in the same proportion. This will lead to an overall multiplicative factor in the right-hand side of rate equation, Eq. (12), modifying the curves in Fig. 9. Besides, our results are strongly dependent on the form factors: Different choices would modify the slope of the curves in Fig. 9. Furthermore, the relevance of the parametrization of the hydrodynamical expansion exhibited in Eq. (14) cannot be underestimated. Different parameters can make the system cool more quickly or slowly and accordingly change the multiplicities of the distinct particles. This was well illustrated in Fig. 12.

V. CONCLUDING REMARKS

In this work, we have analyzed the hadronic effects on the Υ abundance in heavy-ion collisions. Effective Lagrangians have been used to calculate the cross sections for the Υ-production processes $\bar{B}^{(*)} + B^{(*)} \to \Upsilon + (\pi, \rho)$, and also for the corresponding inverse processes associated to the Υ absorption. We have also computed the thermally averaged cross sections for the dissociation and production reactions. Finally, we have employed the thermally averaged cross sections as inputs in the rate equation and have determined the time evolution of the Υ abundance in a hadron gas.

Examining the existing literature on cross-section calculations, the present work has introduced the following improvements: inclusion of reactions which start or end with $\bar{B}B$ and $\bar{B}^*B^*$ in the case of the pion-Υ scattering, and $\bar{B}^*B$ in that involving ρ meson; inclusion of the anomalous parity interactions processes in the effective Lagrangian approach.

Our results suggest that the interactions between Υ and light mesons reduce the Υ abundance at the end of the quark gluon plasma phase.

In conclusion, despite the fact that there are points to be improved to obtain a more realistic description of the HIC phenomenology, we believe that our findings are important for the physics of both the quark gluon plasma and hadronic phases. Our results should encourage further studies of the Υ suppression in the hadron gas phase of relativistic heavy-ion collisions.

ACKNOWLEDGMENTS

The authors would like to thank the Brazilian funding agencies CNPq (Contracts No. 310759/2016-1, No. 311524/2016-8, No. 308088/2017-4, and No. 400546/2016-7, and INCT-FNA), FAPESP (Contract No. 17/07278-5), and FAPESB (Contract No. INT0007/2016) for financial support.

[1] J. Adams, M. M. Aggarwal, Z. Ahammed, J. Amonett, B. D. Anderson, D. Arkhipkin, G. S. Averichev, S. K. Badyal, Y. Bai, J. Balewski *et al.* (STAR Collaboration), Nucl. Phys. A **757**, 102 (2005).

[2] For a recent review, see P. Braun-Munzinger, V. Koch, T. Schafer, and J. Stachel, Phys. Rept. **621**, 76 (2016).

[3] T. Matsui and H. Satz, Phys. Lett. B **178**, 416 (1986).

[4] For a review, see R. Rapp, Prog. Part. Nucl. Phys. **65**, 209 (2010).

[5] A. Andronic, F. Arleo, R. Arnaldi, A. Beraudo, E. Bruna, D. Caffarri, Z. Conesa del Valle, J. G. Contreras, T. Dahms, A. Dainese *et al.*, Eur. Phys. J. C **76**, 107 (2016), and references therein.

[6] R. L. Thews, M. Schroedter, and J. Rafelski, Phys. Rev. C **63**, 054905 (2001); P. Braun-Munzinger and J. Stachel, Phys. Lett. B **490**, 196 (2000).

[7] B. Abelev, J. Adam, D. Adamová, M. M. Aggarwal, G. Aglieri Rinella, M. Agnello, A. G. Agocs, A. Agostinelli, N. Agrawal, Z. Ahammed *et al.* (ALICE Collaboration), Phys. Lett. B **734**, 314 (2014).

[8] J. Adam, D. Adamová, M. M. Aggarwal, G. Aglieri Rinella, M. Agnello, N. Agrawal, Z. Ahammed, S. Ahmad, S. U. Ahn, S. Aiola *et al.* (ALICE Collaboration), Phys. Lett. B **766**, 212 (2017).

[9] W. Zha and Z. Tang, Nucl. Part. Phys. Proc. **289**, 83 (2017).

[10] G. Aarts, J. Aichelin, C. Allton, R. Arnaldi, S. A. Bass, C. Bedda, N. Brambilla, E. Bratkovskaya, P. Braun-Munzinger, G. E. Bruno *et al.*, Eur. Phys. J. A **53**, 93 (2017).

[11] X. Du, M. He, and R. Rapp, Phys. Rev. C **96**, 054901 (2017).

[12] A. Andronic, P. Braun-Munzinger, K. Redlich, and J. Stachel, Phys. Lett. B **652**, 259 (2007); M. I. Gorenstein, A. P. Kostyuk, H. Stoecker, and W. Greiner, *ibid.* **509**, 277 (2001).

[13] Y. Liu, B. Chen, N. Xu, and P. Zhuang, Phys. Lett. B **697**, 32 (2011); K. Zhou, N. Xu, and P. Zhuang, Nucl. Phys. A **931**, 654 (2014).

[14] A. Emerick, X. Zhao, and R. Rapp, Eur. Phys. J. A **48**, 72 (2012).

[15] B. Krouppa and M. Strickland, Universe **2**, 16 (2016).

[16] B. Krouppa, R. Ryblewski, and M. Strickland, Phys. Rev. C **92**, 061901(R) (2015).

[17] Z. Hu, N. T. Leonardo, T. Liu, and M. Haytmyradov, Int. J. Mod. Phys. A **32**, 1730015 (2017).

[18] S. Chatrchyan, V. Khachatryan, A. M. Sirunyan, A. Tumasyan, W. Adam, T. Bergauer, M. Dragicevic, J. Ero, C. Fabjan, M. Friedl *et al.* (CMS Collaboration), Phys. Rev. Lett. **107**, 052302 (2011); Z. Hu, J. Phys. G **38**, 124071 (2011); S. Chatrchyan, V. Khachatryan, A. M. Sirunyan, A. Tumasyan, W. Adam, T. Bergauer, M. Dragicevic, J. Ero, C. Fabjan, M. Friedl *et al.* (CMS Collaboration), J. High Energy Phys. 05 (2012) 063.

[19] L. Adamczyk, J. K. Adkins, G. Agakishiev, M. M. Aggarwal, Z. Ahammed, I. Alekseev, J. Alford, C. D. Anson, A. Aparin, D. Arkhipkin *et al.* (STAR Collaboration), Phys. Lett. B **735**, 127 (2014); **743**, 537(E) (2015).

[20] V. Khachatryan, A. M. Sirunyan, A. Tumasyan, W. Adam, E. Asilar, T. Bergauer, J. Brandstetter, E. Brondolin, M. Dragicevic, J. Erö *et al.* (CMS Collaboration), Eur. Phys. J. C **77**, 252 (2017).

[21] A. M. Sirunyan, A. Tumasyan, W. Adam, F. Ambrogi, E. Asilar, T. Bergauer, J. Brandstetter, E. Brondolin, M. Dragicevic, J. Ero *et al.* (CMS Collaboration), Phys. Lett. B **790**, 270 (2019).

[22] V. Khachatryan, A. M. Sirunyan, A. Tumasyan, W. Adam, E. Asilar, T. Bergauer, J. Brandstetter, E. Brondolin, M. Dragicevic, J. Ero *et al.* (CMS Collaboration), Phys. Lett. B **770**, 357 (2017).

[23] V. Khachatryan, A. M. Sirunyan, A. Tumasyan, W. Adam, E. Asilar, T. Bergauer, J. Brandstetter, E. Brondolin, M. Dragicevic, J. Ero *et al.* (CMS Collaboration), Phys. Lett. B **04**, 031 (2017).

[24] V. M. Shapoval, P. Braun-Munzinger, and Y. M. Sinyukov, Nucl. Phys. A **968**, 391 (2017).

[25] J. Adam, D. Adamová, M. M. Aggarwal, G. Aglieri Rinella, M. Agnello, N. Agrawal, Z. Ahammed, S. Ahmad, S. U. Ahn, S. Aiola *et al.* (ALICE Collaboration), Phys. Rev. C **95**, 064606 (2017).

[26] B. Abelev, J. Adam, D. Adamová, M. M. Aggarwal, M. Agnello, A. Agostinelli, N. Agrawal, Z. Ahammed, N. Ahmad, A. Ahmad Masoodi *et al.* (ALICE Collaboration), Phys. Rev. C **91**, 024609 (2015).

[27] V. G. Riabov (ALICE Collaboration), J. Phys. Conf. Ser. **798**, 012054 (2017); C. Markert (ALICE Collaboration), *ibid.* **878**, 012003 (2017).

[28] L. M. Abreu, K. P. Khemchandani, A. M. Torres, F. S. Navarra, and M. Nielsen, Phys. Rev. C **97**, 044902 (2018).
[29] S. G. Matinyan and B. Müller, Phys. Rev. C **58**, 2994 (1998); A. Bourque and C. Gale, *ibid.* **80**, 015204 (2009); **78**, 035206 (2008); A. Bourque, C. Gale, and K. L. Haglin, *ibid.* **70**, 055203 (2004); Z. Lin and C. M. Ko, *ibid.* **62**, 034903 (2000); J. Phys. G **27**, 617 (2001); F. S. Navarra, M. Nielsen, and M. R. Robilotta, Phys. Rev. C **64**, 021901(R) (2001); K. L. Haglin and C. Gale, *ibid.* **63**, 065201 (2001); K. L. Haglin, *ibid.* **61**, 031902 (2000); F. Carvalho, F. O. Duraes, F. S. Navarra, and M. Nielsen, *ibid.* **72**, 024902 (2005).
[30] Y. Oh, T. Song, and S. H. Lee, Phys. Rev. C **63**, 034901 (2001).
[31] K. P. Khemchandani, A. Martinez Torres, M. Nielsen, and F. S. Navarra, Phys. Rev. D **89**, 014029 (2014).
[32] F. O. Durães, H. Kim, S. H. Lee, F. S. Navarra, and M. Nielsen, Phys. Rev. C **68**, 035208 (2003); F. O. Duraes, S. H. Lee, F. S. Navarra, and M. Nielsen, Phys. Lett. B **564**, 97 (2003); F. S. Navarra, M. Nielsen, R. S. Marques de Carvalho, and G. Krein, *ibid.* **529**, 87 (2002).
[33] E. G. Ferreiro and J. P. Lansberg, J. High Energy Phys. 10 (2018) 094.
[34] Z. Lin and C. M. Ko, Phys. Lett. B **503**, 104 (2001).
[35] H. Nagahiro, L. Roca, and E. Oset, Eur. Phys. J. A **36**, 73 (2008).
[36] A. Martinez Torres, K. P. Khemchandani, F. S. Navarra, M. Nielsen, and L. M. Abreu, Phys. Rev. D **90**, 114023, (2014); **93**, 059902(E) (2016).
[37] L. M. Abreu, K. P. Khemchandani, A. Martinez Torres, F. S. Navarra, and M. Nielsen, Phys. Lett. B **761**, 303 (2016).
[38] B. C. Pearce and B. K. Jennings, Nucl. Phys. A **528**, 655 (1991).
[39] Y. S. Oh, T. S. Song, S. H. Lee, and C. Y. Wong, J. Korean Phys. Soc. **43**, 1003 (2003).
[40] D. Ronchen, M. Doring, F. Huang, H. Haberzettl, J. Haidenbauer, C. Hanhart, S. Krewald, U.-G. Meissner, and K. Nakayama, Eur. Phys. J. A **49**, 44 (2013).
[41] M. E. Bracco, M. Chiapparini, F. S. Navarra, and M. Nielsen, Prog. Part. Nucl. Phys. **67**, 1019 (2012).
[42] P. Koch, B. Muller, and J. Rafelski, Phys. Rep. **142**, 167 (1986).
[43] S. Cho, T. Furumoto, T. Hyodo, D. Jido, C. M. Ko, S. H. Lee, M. Nielsen, A. Ohnishi, T. Sekihara, S. Yasui, and K. Yazaki (ExHIC Collaboration), Phys. Rev. Lett. **106**, 212001 (2011).
[44] S. Cho and S. H. Lee, Phys. Rev. C **97**, 034908 (2018).
[45] S. Cho, T. Furumoto, T. Hyodo, D. Jido, C. M. Ko, S. H. Lee, M. Nielsen, A. Ohnishi, T. Sekihara, S. Yasui, and K. Yazaki (ExHIC Collaboration), Phys. Rev. C **84**, 064910 (2011).
[46] S. Cho, T. Hyodo, D. Jido, C. M. Ko, S. H. Lee, S. Maeda, K. Miyahara, K. Morita, M. Nielsen, A. Ohnishi, T. Sekihara, T. Song, S. Yasui, and K. Yazaki (ExHIC Collaboration), Prog. Part. Nucl. Phys. **95**, 279 (2017).
[47] L. W. Chen, C. M. Ko, W. Liu, and M. Nielsen, Phys. Rev. C **76**, 014906 (2007).
[48] S. Cho and S. H. Lee, Phys. Rev. C **88**, 054901 (2013).
[49] C. M. Ko, V. Koch, Z.-W. Lin, K. Redlich, M. Stephanov, and X.-N. Wang, Phys. Rev. Lett. **86**, 5438 (2001).